Energy-Efficient Link Resource Allocation in the Multibeam Satellite Downlink under QoS Constraints

R. Andreotti[1,2], F. Giannetti[1*], and M. Luise[1]

[1] *Department of Information Engineering, University of Pisa, Via G. Caruso 16, I-56122, Italy.*
[2] *Wireless Systems Engineering and Research (WISER) S.r.l., Via Fiume 23, Livorno, I-57123, Italy.*

SUMMARY

This work deals with the issue of boosting the capacity of xDSL networks in the presence of geographical gaps. To this aim, an effective approach consists in exploiting the downlink of multibeam satellites for the delivering of packed-based traffic, employing modulation and coding schemes denoted by very high spectral efficiency, such as in DVB-S2X standard. Though, time-varying channel and interference may severely affect the quality of the communication. To cope with these issues, this paper proposes a novel link resource adaptation based on the following features. First, to efficiently manage packet-based transmissions, an adaptive coding and modulation (ACM) scheme is derived aimed at maximizing the "goodput" (GP), i.e., the offered layer-3 data rate. Then, in order to mitigate the co-channel interference arising from beams exploiting the same band, an adaptive power control (PC) is also proposed. The goal of the latter is to maximize the energy-efficiency of the satellite downlink guaranteeing a given quality-of-service, i.e., a minimum-GP, over each link. This problem is modeled as a non-cooperative game and the conditions of feasibility, existence and uniqueness of the solution are analytically derived. Finally, simulation results are provided comparing the proposed strategy with the conventional rate satisfaction PC approach.

KEY WORDS: ACM; power control; energy-efficiency; goodput

1. INTRODUCTION

The ever increasing demand for broadband Internet opens up new fecund opportunities for next generation satellite systems. Indeed, even though high-speed and reliable connections, both wired and wireless, are commonly available in urban areas, there still remain many other scenarios that could continue suffering from limited connectivity, even in the next future. Rural and scarcely inhabited areas, as well as a plethora of entities typically located in sub-urban areas, such as government agencies, large multinational companies and international organizations, which need high-speed connections all over the world for communicating with company premises (i.e.,

*Correspondence to: filippo.giannetti@iet.unipi.it.

headquarters, offices, factories, warehouses, retailers, etc.) with business partners, and with a growing number of home-based telecommuters, are only a few of those situations.

All of these examples justify the need of resorting to multibeam geostationary Earth orbit (GEO) satellite to boost the (often limited) downstream capacity of xDSL (Digital Subscriber Line) terrestrial networks. Multibeam GEO satellite represents in fact the most effective medium capable of providing ubiquitous broadband downstream connections over large geographical areas: narrow beams can allow for a higher power density than broad beams, enabling therefore higher data rates at ground-based user terminals (UTs). Moreover, the total downlink capacity can be further enhanced by exploiting higher frequency bands, such as Ka-band and beyond [1], and by reusing either the same frequencies in different beams and the same frequency with different polarizations within the same beam. Such a kind of hybrid satellite/xDSL network, providing the users with higher data rates thanks to an additional on-demand downstream via satellite connection, could rely on either legacy broadcast DVB-S2/DVB-S2X (Digital Video Broadcasting-Satellite, version 2 and eXtension) [2] or a next generation satellite with multiple beams and operating in high frequency bands.

In the scenario depicted above, the quality of the downlink signals aimed at UTs located inside a given beam can be significantly affected by several highly time-variant factors. Among these, let recall here the channel variability caused by atmospheric impairments, such as rain fading, the random nature of both traffic data inside the beam and interference originated from signals that are radiated in other beams re-using the same frequency band and polarization. As a consequence, in order to cope with these detrimental effects, the available physical layer resources must be efficiently allocated over the downlink transmission. Such link adaptation (LA) policies allow the update of the transmitted signal according to the varying channel and interference conditions ensuring to the UTs a given quality of service (QoS).

One simple LA strategy is the adaptive coding and modulation (ACM) which consists in the selection of the "modulation order/coding rate" (MC) pair that is best suited for the current channel/interference conditions. It is worthwhile to note that ACM is also part of the DVB-S2X standard providing support to the downlink of interactive services via satellite [2]. Several works deal with the investigation of the ACM problem for satellite communications. In [3, 4] the chosen tupla modulation order, coding rate and spreading factor is the one maximizing the spectral efficiency under the requirement that the signal-to-noise-plus-interference ratio (SINR) is above a given threshold. In [5], the ACM mode is selected based on a quantization, depending on the number of available modulation order/coding rate pairs, of the instantaneous bit rate, whereas the work in [6] considers ACM in combination with dynamic rate adaptation. Another LA policy usually employed is the power control (PC) mechanism, which sets the level of power of the transmitted signals in order to meet a given QoS requirement per UT, in terms of SINR or data rate. This technique is particularly suitable to counteract the co-channel interference arising in multibeam downlink, as shown in [7], where a satellite CDMA network is considered, and in [8, 9] where the power is jointly optimized with the carrier allocation and beamforming, respectively.

The present paper focuses on the satellite downlink of a hybrid satellite/xDSL network which boosts the capacity of the downstream link towards the UTs and proposes a novel ACM and PC scheme for next generation Ka-band multibeam satellite. Several innovative contributions distinguish our work from the literature and can be summarized as reported hereafter. First, since the system deals with packet-based transmissions, the spectral efficiency over each link is suitably

expressed by the offered layer-3 data rate, also termed "goodput" (GP) for short, representing the number of bits transported by successfully delivered packets per unit of time, net of overheads [10]. Then, a novel ACM scheme that maximizes the GP of the proposed system is provided. To this aim, the look-up table (LUT) for ACM is numerically derived by associating to any SINR of the satellite downlink, the MC pair yielding the highest value of GP. Besides, the system is based on DVB-S2X signal format, which further boosts the spectral efficiency by employing modulation orders up to 256-APSK combined with proper low density parity check (LDPC) block codes. Next, in order to manage the co-channel interference arising from beams exploiting the same band, an adaptive PC algorithm is also proposed. In particular, unlike conventional PC strategies discussed above and taking into account the recent works in [11] and [12] about energy-efficiency (EE) for wireless networks, we extend this framework to the downlink multibeam satellite transmission context. Hence, it is proposed and investigated a novel PC algorithm that maximizes the EE of the system while guaranteeing a given QoS over each link in terms of minimum-GP constraint. The PC problem is studied resorting to the non-cooperative game theory framework [13], which provides an effective tool to investigate the existence and uniqueness of the solution. We further provide more insight on the impact the QoS constraints and the possible maximum transmission power constraint have on the feasibility of the problem and how they affect structure of the PC algorithm, as well as on the physical meaning of the proposed EE approach compared with conventional PC policy based only on rate or SINR constraint satisfaction. Finally, the effectiveness of the proposed ACM and PC schemes is assessed by numerical simulations.

Notations. Matrices (vectors) are in upper (lower) case bold, calligraphic mathematical symbols, e.g., $\mathcal{A}$, represent sets, $[\cdot]^T$ is the transpose operator, $\times$ denotes the Cartesian product, $\|\mathbf{a}\| \triangleq \sqrt{\mathbf{a}^T\mathbf{a}}$ is the ℓ_2-norm of vector $\mathbf{a}$, $x \in \mathcal{CN}(0, \sigma^2)$ is a zero-mean Gaussian complex random variable (RV) with variance σ^2.

2. SYSTEM MODEL

This work focuses on the hybrid terrestrial-satellite network, shown in Fig. 1. The xDSL connection shown in the figure supports the upstream from the UTs to the terrestrial ISP, but it is assumed that the xDSL downstream is inadequate due to poor quality and/or limited capacity. In the proposed solution, a gateway station feeds a bent-pipe geostationary satellite whose downlink boosts the downstream capacity of the UTs. In the following, we illustrate the satellite downlink which shall satisfy the users' QoS requirements, and, in the next section, we will analyze the relevant performance.

2.1. Multibeam configuration

We consider a multibeam downlink featuring N_b beams belonging to the set $\mathcal{B}$. We use the term "color" to designate a pair made of a frequency band and a polarization, e.g., horizontal (H) or vertical (V), that are assigned to each beam, and we assume a "colored" transmission scheme based on both frequency and polarization reuse. Fig. 2 depicts an example of a 4-color multibeam European coverage. Denoting with N_p the number of polarizations and with and N_sb the number of contiguous frequency subbands the overall available band is split, the number of available colors

)
t

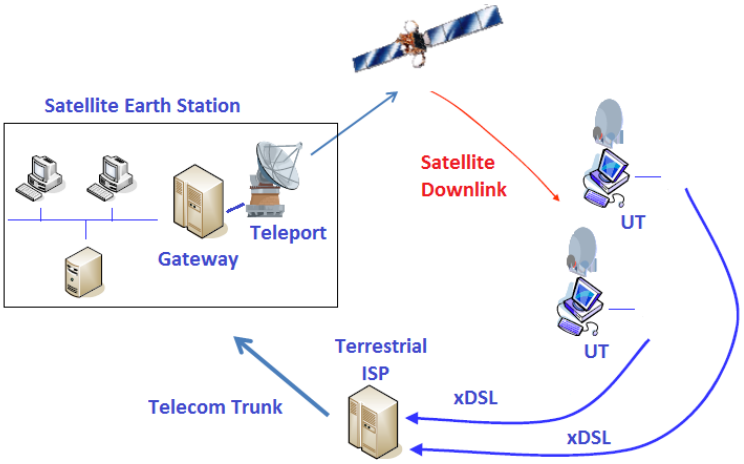

Figure 1. System architecture as provided by [14].

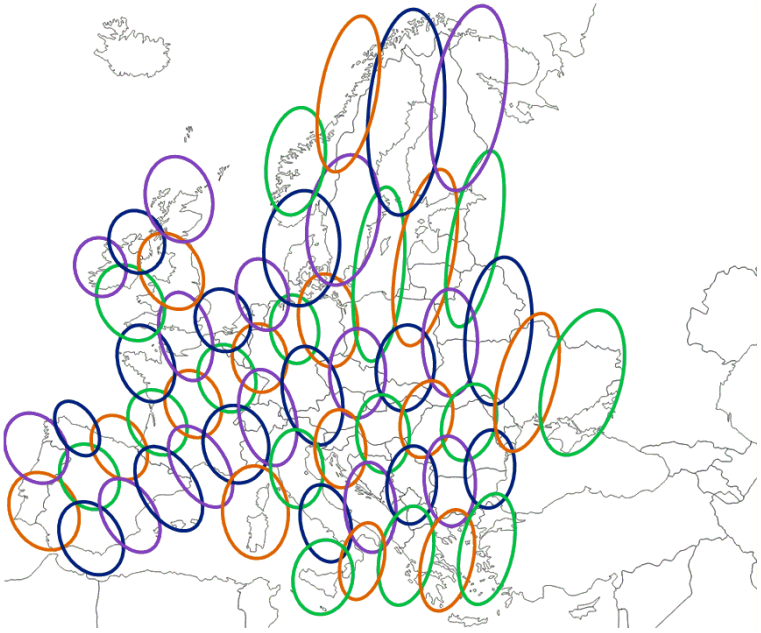

Figure 2. European coverage provided by a 4-color multibeam satellite.

turns out $C = N_{\mathrm{sb}} \cdot N_{\mathrm{p}}$. Each UT is served by one beam and is tuned on a frequency carrier, with the proper polarization, belonging to the frequency subband which is associated to that beam. Now, let $\mathcal{Q}_c \subseteq \mathcal{B}$ be the Q-sized subset of the satellite beams containing only those beams sharing the color $c \in \{1, \cdots, C\}$, i.e., the same frequency band and polarization pair. Assuming w.l.g. that N_{b} is an integer multiple of C, the number of beams sharing the same color results $Q = N_{\mathrm{b}}/C$. The quality of the received signal at the generic UT located in the generic beam $q \in \mathcal{Q}_c$ is measured by the SINR, where the interference originates, through the side lobes of the satellite antennas, from the power leakage of the signals that are radiated in the other $Q - 1$ beams with the same color, which belong thus to the complementary set $\overline{\mathcal{Q}_c} \triangleq \mathcal{Q}_c/\{q\}$.

2.2. *Physical layer*

Let us consider the downlink of a multibeam satellite, compliant with the DVB-S2X standard [2], whose main parameters are listed in Tab. I, and let us focus, w.l.g., on the received signal within the generic beam $q \in \mathcal{Q}_c$, $\forall c \in \{1, \cdots, C\}$. Thus, for the sake of readability, from now on we will drop the color index c. Besides, Fig. 3 depicts the equivalent block scheme of the physical layer processing for the considered satellite downlink, described in the following.

Parameter	Value
BB Header Length $N^{(\mathrm{bb_{hdr}})}$	80 bits
FEC Frame Length $n^{(\mathrm{ldpc})}$	64800 bits
Set of Bits per Modulation Symbol $\mathcal{D}_{\mathrm{m}}$	$\{2, 3, 4, 5, 6, 7, 8\}$
Set of Coding Rates $\mathcal{D}_{\mathrm{r}}$	$\{\frac{3}{5}, \frac{2}{9}, \frac{13}{45}, \frac{9}{20}, \frac{90}{180}, \frac{96}{180}, \frac{11}{20}, \frac{100}{180}, \frac{104}{180}, \frac{2}{3}, \frac{26}{45}, \frac{18}{30}, \frac{28}{45}, \frac{23}{36}, \frac{116}{180}, \frac{20}{30}, \frac{124}{180}, \frac{25}{36}, \frac{4}{5}, \frac{5}{6}, \frac{128}{180}, \frac{13}{18}, \frac{132}{180}, \frac{22}{30}, \frac{135}{1580}, \frac{140}{180}, \frac{7}{9}, \frac{154}{180}\}$
PL Slot Length S	90 modulation symbols

Table I. Parameters values of DVB-S2X standard.

At the ground transmitter side (i.e., at the gateway), a header of $N_q^{(\mathrm{bb_{hdr}})}$ bits is appended to any information-bearing data packet, consisting of $k_q^{(\mathrm{bch})} - N_q^{(\mathrm{bb_{hdr}})}$ bits, which is coming from the upper layers. The resulting base band (BB) frame is then sent to the forward error correction (FEC) encoder, which is made of the concatenation of an outer BCH (Bose-Chaudhuri-Hocquenghem) encoder and an inner LDPC (low-density parity-check) encoder. The BCH encoder is a cyclic block code identified by the pair $(k_q^{(\mathrm{bch})}, n_q^{(\mathrm{bch})})$, yielding a coding rate $r_q^{(\mathrm{bch})} = k_q^{(\mathrm{bch})}/n_q^{(\mathrm{bch})}$. The $n_q^{(\mathrm{bch})}$ coded binary symbols (CBS) output by the BCH encoder are then sent to the subsequent LDPC encoder, which produces a fixed-length output of $n_q^{(\mathrm{ldpc})}$ CBS, referred to as FEC frame. The LDPC block has therefore a coding rate of $r_q^{(\mathrm{ldpc})} = n_q^{(\mathrm{bch})}/n_q^{(\mathrm{ldpc})}$, so that the overall coding rate results $r_q = r_q^{(\mathrm{bch})} \cdot r_q^{(\mathrm{ldpc})}$, with $r_q \in \mathcal{D}_{\mathrm{r}}$, being $\mathcal{D}_{\mathrm{r}}$ the set of allowed coding rates. Eventually, the $n_q^{(\mathrm{ldpc})}$ CBS are interleaved and then mapped into a sequence of N_q unit-energy modulation symbols $\{x_{q,n}\}_{n=1}^{N_q}$ belonging to a 2^{m_q}-sized PSK or APSK constellation, with $N_q \triangleq n_q^{(\mathrm{ldpc})}/m_q$, being $m_q \in \mathcal{D}_{\mathrm{m}}$ the number of label bits per modulation symbol and $\mathcal{D}_{\mathrm{m}}$ the set of bits per PSK/APSK modulation symbol. These symbols are grouped into slots, each one containing S symbols, which are encapsulated into the physical layer (PL) frame along with the PL header made of S $\pi/2$-BPSK symbols, containing information on the chosen modulation and coding pair, on the length of the FEC frame, and, possibly, on the pilot symbols for carrier recovery. Finally, the symbols of the PL frame are filtered by the BB filter and uplinked to the satellite, which retransmits the signal in beam q with power $p_q \leq p_q^{(\max)}$, where $p_q^{(\max)}$ is the maximum power of the transponder. The model of the data symbol received by a UT in beam q can thus be written as

$$y_q = \sqrt{p_q} h_{q,q} x_q + \sum_{t=1,\, t\neq q}^{Q} \sqrt{p_t} h_{t,q} x_t + w_q, \tag{1}$$

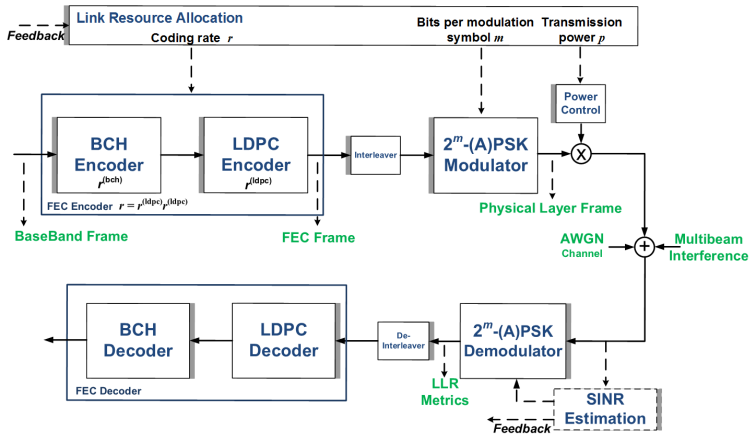

Figure 3. Equivalent block scheme of the physical layer for the considered satellite downlink.

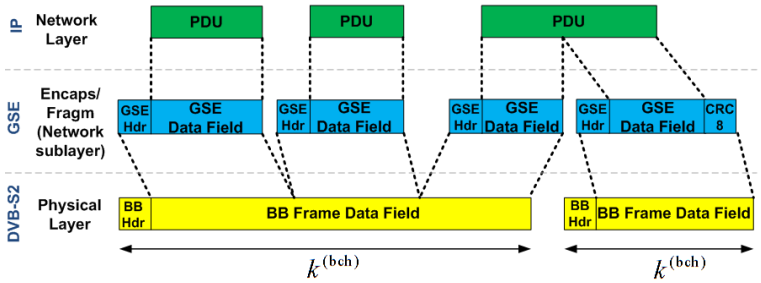

Figure 4. Example of the GSE scheme.

where $w_q \in \mathcal{CN}(0, \sigma_q^2)$ denotes the noise and we defined $h_{i,j} \triangleq \sqrt{g_{i,j}/l_j}$, being $g_{i,j}$ the antenna gain from the emitting antenna of beam i toward the UT located in beam j, and l_j the overall path loss (including free-space propagation and atmospheric loss, space and ground system impairments, ground antenna gain) between the satellite and the UT in beam j. The received signal is finally demodulated and decoded and, given a selection of modulation order and coding rate, the probability of successful reception of information-bearing data by the UT in beam q depends on the SINR which, according to (1), can be expressed as

$$\gamma_q = \frac{p_q |h_{q,q}|^2}{\sigma_q^2 + \sum\limits_{t=1,\, t\neq q}^{Q} p_t |h_{t,q}|^2}. \tag{2}$$

2.3. *GSE protocol*

First generation (DVB-S) only supports audio/video streams in MPEG format by adopting Transport Stream (TS) packet multiplexing, wherein the packets are characterized by fixed length and specific QoS constraints. Second generation (DVB-S2 and its extension DVB-S2X), besides offering backwards compatibility for MPEG-TS, also provides a novel protocol to support Generic Streams, i.e., variable-length streams, without specific timing/rate constraints [14, 15]. This protocol, called generic stream encapsulation (GSE), fragments the IP (Internet Protocol) data packets to fill the

entire data field of the BB frame with no need of padding and with a minimum amount of overhead. Fig. 4 shows an example of the encapsulation scheme of the GSE protocol. As apparent many layer-3 protocol data units (PDUs), corresponding to the data requested by the generic UT via xDSL upstream and routed to the gateway as depicted in Fig. 1, are encapsulated into GSE frames as required to fill the BB frame data field, by appending a header of 10 bytes at most to each of them. In the following, we assume full buffer per UT, so that every BB frame is filled with PDUs associated to only one UT.

3. ACM SCHEME FOR GOODPUT OPTIMIZATION

This section describes rationale of the ACM scheme, i.e., the strategy for the selection of the best pair of coding rate and modulation order, to be employed in the downlink by the carrier serving an UT inside beam q. Dropping the dependence on the beam index q, for the sake of notation simplicity, let us assume that the UT is experiencing a SINR γ.

The data packets are identified by the PDUs encapsulated into the GSE packets, contained, in turn, into the BB frame for transmission, as described in Sect. 2.3. The GP metric is given by the ratio between the number of transmitted information bits and the time required to successfully receive them, which, in turns, depends on the time duration of the frame related to the choice of the transmission parameters [10]. Considering a bit rate R_b and a matched filter at receiver over the band $B = 1/R_b$, the normalized GP, i.e., the number of correctly received PDU's information bits per second per Hz, can be expressed as [10]

$$\zeta(r, m|\gamma) = \zeta_0 \cdot r \cdot m \cdot [1 - \phi_r(m|\gamma)], \quad (\text{bit/s/Hz}) \tag{3}$$

where $\zeta_0 = (k^{(\text{bch})} - N^{(\text{bb}_{\text{hdr}})} - N^{(\text{gse})})/k^{(\text{bch})}$, with $N^{(\text{bb}_{\text{hdr}})}$ and $N^{(\text{gse})}$ denoting the length in bits of the BB frame and the GSE headers, respectively, accounts for the loss of efficiency due to the GSE and BB headers, and $\phi_r(m|\gamma)$ is the frame error rate (FER), which describes the probability of erroneously receiving the BB frame when a modulation with a 2^m-sized constellation is employed along with code rate r, at a given SINR value γ. The ACM problem can thus be stated as

$$\begin{aligned} (r^*, m^*) = \quad & \arg\max_{(r,m)} \zeta(r, m|\gamma) \\ \text{s.t.} \quad & (r, m) \in \mathcal{D}_\text{r} \times \mathcal{D}_\text{m} \end{aligned} . \tag{4}$$

Unfortunately, there is not an exact closed-form expression of the coded FER $\phi_r(\cdot)$ yielding an analytical expression that relates the optimal MC pair (r^*, m^*) to the corresponding SINR γ. Thus, for any pair (r, m), the FER values are evaluated as a function of γ by resorting to a Monte Carlo simulation and stored into a LUT. Then, problem (4) is solved via a simple exhaustive search on the small-sized set $\mathcal{D}_\text{r} \times \mathcal{D}_\text{m}$. Moreover, the DVB-S2X standard further reduces the size of this set, since it allows the adoption of only 39 pairs out of all the possible MC combinations [2]. Fig. 5 depicts the GP curves, obtained by computer simulation with 1500-byte PDUs and averaging over 10^3 independent BB frames, as a function of the SINR γ. The following remarks are in order.

i) The spectral efficiency of the system is represented by the envelope of the GP curves in Fig. 5.

ii) In the figure, there are depicted only 30 curves, out of 39 possible pairs (r, m) associated to

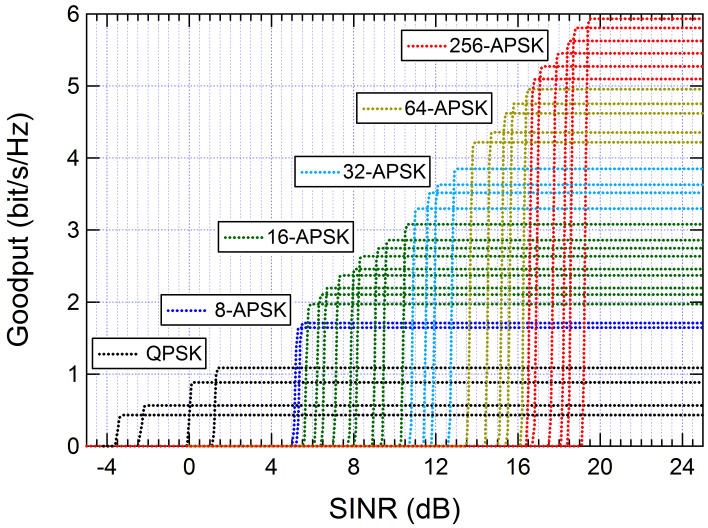

Figure 5. Goodput performance of DVB-S2X static modes.

normal FEC frames in the DVB-S2X standard [2, Tab. 20a], since some pairs produce GP curves that always lie under the envelope of the whole curve set.

iii) The values of γ relevant to the crossing points of the curves represent the SINR thresholds of the LUT, whose entries are reported in Tab. II, and drive the selection of the pair (r, m) yielding the best GP performance.

iv) The UT measures the received SINR γ and, thanks to the LUT, selects the pair (r, m) providing the best GP performance. Then, an index in the set $\{1, 2, \ldots, 30\}$, representing the chosen pair, is sent to the transmit gateway via the terrestrial xDSL-based return channel, thus enabling the interactivity between the UT and the gateway.

v) The spectral efficiency represented by the envelope of the curves in Fig. 5 can be effectively approximated by the following closed-form expression

$$\eta(\gamma) = \log_2\left(1 + \frac{\gamma}{\Gamma}\right), \tag{5}$$

where $\Gamma > 1$ is the SINR gap [16, 17] between the channel capacity and the actual spectral efficiency of the system employing practical modulation and coding schemes. For the considered MC pairs, the value of the SINR gap is $\Gamma = 1.448$ and has been evaluated by minimizing the mean quadratic error between (5) and the envelope of the GP curves of Fig. 5.

4. ENERGY-EFFICIENT POWER OPTIMIZATION

In the scenario under analysis, the generic UT in beam q is denoted by a certain QoS requirement, expressed in terms of a minimum GP $\bar{\eta}_q$ to satisfy on the satellite downlink. Though, the co-channel interference coming from the on-board antennas transmitting towards beams using the same color as beam q (i.e., exploiting the same band and polarization), can degrade the signal quality at the UT, as shown in eqn. (1). Thus, on the one hand, this calls for the necessity of an effective PC algorithm able to satisfy the QoS of every UT. On the other hand, one should also look at the overall

Modulation and Coding Scheme	SINR Threshold (dB)	Modulation and Coding Scheme	SINR Threshold (dB)
$4-$PSK $2/9$	-3.7	$32-$APSK $2/3$	10.98
$4-$PSK $13/45$	-2.25	$32-$APSK $128/180$	11.6
$4-$PSK $9/20$	0.03	$32-$APSK $132/180$	12.05
$4-$PSK $11/20$	1.27	$32-$APSK $140/180$	12.88
$8-$APSK $100/180$	5.17	$64-$APSK $128/180$	13.77
$8-$APSK $104/180$	5.47	$64-$APSK $132/180$	14.66
$16-$APSK $90/180$	5.77	$64-$APSK $140/180$	15.3
$16-$APSK $96/180$	6.32	$64-$APSK $4/5$	15.74
$16-$APSK $100/180$	6.68	$64-$APSK $5/6$	16.40
$16-$APSK $18/30$	7.25	$256-$APSK $116/180$	16.73
$16-$APSK $28/45$	7.98	$256-$APSK $20/30$	17.08
$16-$APSK $20/30$	8.29	$256-$APSK $124/180$	17.87
$16-$APSK $25/36$	9.14	$256-$APSK $128/180$	18.40
$16-$APSK $13/18$	9.59	$256-$APSK $22/30$	18.70
$16-$APSK $140/180$	10.49	$256-$APSK $135/180$	19.40

Table II. Table of ACM for Goodput Optimization based on DVB-S2X MC pairs.

energy efficiency of the satellite, since a non-negligible amount of power P_c is consumed to feed the transponder and all the on-board electronic devices. Therefore, with the aim of minimizing the waste of energy, inspired by the recent works in wireless networks [11, 12], we propose to allocate the transmit power in order to maximize the EE of the system, expressed in bit/s/Hz/J. Indeed, to the best of authors' knowledge, the scenario at hand, which differs from those in [11, 12] for assumptions and operating conditions, still lacks of an EE analysis, that will be the subject of this section.

In particular, Sect. 4.1 formalizes the EE problem over the satellite downlink, whereas Sect. 4.2 and Sect. 4.3 provide the tools for its analysis and solution.

4.1. Problem formulation

In order to introduce the EE optimization problem, consider the UT located in beam $q \in \mathcal{Q}$. Then, the figure of merit describing the EE over the downlink between the transponder and the UT is expressed by

$$u_q(\mathbf{p}) \triangleq \frac{\eta_q(\mathbf{p})}{P_c + p_q} = \frac{\log_2\left(1 + \frac{\gamma_q(\mathbf{p})}{\Gamma}\right)}{P_c + p_q}, \tag{6}$$

where the dependence of the quantities of interest on the power allocation vector $\mathbf{p} \triangleq [p_1, \cdots, p_q, \cdots, p_Q]^T$ across the iso-color beams is now made explicit. Expression (6) yields the

following multibeam downlink EE optimization problem:

$$\begin{aligned} \mathbf{p}^* = \arg\max_{\mathbf{p}} \quad & \sum_{q=1}^{Q} u_q(\mathbf{p}) \\ \text{s.t.} \quad & 0 \le p_q \le p_q^{(\max)}, \quad \forall q \in \mathcal{Q}, \\ & \eta_q(\mathbf{p}) - \bar{\eta}_q \ge 0, \quad \forall q \in \mathcal{Q}, \end{aligned} \tag{7}$$

A close look at this problem reveals that both the objective function and the left-hand side of the QoS constraint are non-convex functions of the PA vector and, as a consequence, the overall optimization problem (7) is non-convex. The solution set may be empty, in that there may not be a PA vector value satisfying all the constraints simultaneously, or even composed by multiple local optima [18]. Besides finding, among these, the global optimum results difficult. Nevertheless, there can be found in the literature several techniques that allow to find a feasible solution to this kind of problems, for instance by means of iteratively improving local optima found by proper convex relaxations of the problem or by means of global optimization algorithms [19]. For the case at hand, it can be noted that (7) entails a competition for the frequency resources to be shared over the downlink between the transponders and the UTs. Indeed, the higher the power allocated over a given frequency, the higher the rate obtained at the relevant UT, but the higher the interference caused to the other UTs tuned over the same frequency. This consideration paves the way to a different but effective interpretation of the problem, by modeling it in the framework of non-cooperative game theory [13]. The latter in fact offers an analytical tool that describes how rational entities interact and make appropriate choices so as to find their own maximum utility.

Accordingly, by introducing the complementary power vector w.r.t. beam q as $\mathbf{p}_{-q} \triangleq [p_1, \cdots, p_{q-1}, p_{q+1}, \cdots, p_Q]^T$, the non-cooperative game $\mathcal{G}$ associated to the multibeam EE problem is identified, in strategic form, by the tupla $\{\mathcal{Q}, \mathcal{P}, \{u_q\}_q^{\mathcal{Q}}\}$, where

- $\mathcal{Q} \triangleq \{1, \cdots, Q\}$ denotes the set of players, corresponding to the set of transponders tuned on the same frequency and polarization and transmitting to different UTs (with a slight abuse of vocabulary, it corresponds to the set of beams with the same color);
- $\mathcal{P} = \mathcal{P}_1 \times \cdots \times \mathcal{P}_Q$ is the set of strategies, defined by the Cartesian product of the set of the strategies
$$\mathcal{P}_q(\mathbf{p}_{-q}) \triangleq \{p_q | \eta_q(p_q, \mathbf{p_{-q}}) \ge \bar{\eta}_q,\ 0 \le p_q \le p_q^{(\max)}\}, \tag{8}$$
of every player $q \in \mathcal{Q}$, that is, the set of feasible power values of p_q satisfying constraints in (7);
- u_q is the player $q \in \mathcal{Q}$ payoff function, corresponding to the EE function defined in (6).

Thus, the game can be formally described as[†]

$$\mathcal{G}: \begin{array}{ll} \max\limits_{p_q} & u_q(p_q, \mathbf{p}_{-q}) \\ \text{s.t.} & p_q \in \mathcal{P}_q(\mathbf{p}_{-q}), \end{array} \quad \forall q \in \mathcal{Q}. \tag{9}$$

[†]In the following, we will interchangeably represent the power vector either as $\mathbf{p}$ or as $(p_q, \mathbf{p}_{-q})$, depending on the case at hand.

It is worth noting that, in this case, not only the payoff function, but also the set of strategies of a given player q depends on the other players strategies $\mathbf{p}_{-q}$. When this happens, the solution of the game is investigated in terms of generalized Nash equilibrium (GNE), that collects all system states that are stable to unilateral deviations, or, in other words, the situation where no player gets an increment of its payoff by changing its strategy unless the other players change their strategies too [13]. Moreover, looking at (9), it is evident that the problem may be unfeasible, in that there may not exist a power vector $\mathbf{p}$ able to satisfy all the constraints at the same time.

Finally, it is worth remarking the following observation about the formalization of the EE problem as a non-cooperative game. Usually, in wireless networks, such problems are associated to distributed scenarios, where, for instance, the players are mobile terminals which update their power levels, i.e. strategies, by means of a distributed algorithm until the equilibrium of the game is reached. Here instead, we are dealing with a centralized scenario where, as shown in the following section, the GNE is actually obtained by an iterative algorithm which is run by a central entity (e.g., the gateway) requiring a reasonable amount of information about the satellite multibeam downlink. Anyway, the formalization of the problem as a non-cooperative game is employed, w.l.g., since it simplifies the study of the problem, providing effective tools to analyze the conditions of existence and uniqueness of the solution, as well as to derive the iterative algorithm to reach such a solution.

4.2. Best-response solution

In order to study game $\mathcal{G}$, let us assume it is feasible and introduce the best-response of the generic player q. The latter is nothing but the best power level a rational self-optimizing player can choose in response to the powers actually chosen by other players [20]. Thus, for the moment we consider that for player q the optimal power allocation p_q^* is such that $p_q^* \leq p_q^{(\max)}$ and as a consequence we neglect the maximum power constraint. The impact of the latter will be taken into account in the following section.

Lemma 1. For a fixed strategy $\mathbf{p}_{-q}$ of the other players, the solution of (9) is unique and is given by

$$p_q^* = f_{\mathrm{BR}}\left(\mathbf{p}_{-q}\right) = \frac{\gamma_q^*(\mathbf{p}_{-q})}{\mu_q(\mathbf{p}_{-q})} \quad \forall q \in \mathcal{Q}, \tag{10}$$

where $f_{\mathrm{BR}}(\cdot)$ is the best-response function, $\boldsymbol{\mu} \triangleq [\mu_1, \cdots, \mu_Q]$, where

$$\mu_q \triangleq \frac{\gamma_q}{p_q} = \frac{|h_{q,q}|^2}{\sigma_q^2 + \sum\limits_{t=1,\, t\neq q}^{Q} p_t |h_{t,q}|^2}, \tag{11}$$

is the carrier-to-interference-plus-noise ratio (CINR) vector and

$$\gamma_q^*(\mathbf{p}_{-q}) = \max\{\bar{\gamma}_q, \tilde{\gamma}_q(\mathbf{p}_{-q})\}, \tag{12}$$

with

$$\bar{\gamma}_q \triangleq \Gamma(2^{\bar{\eta}_q} - 1) \tag{13}$$

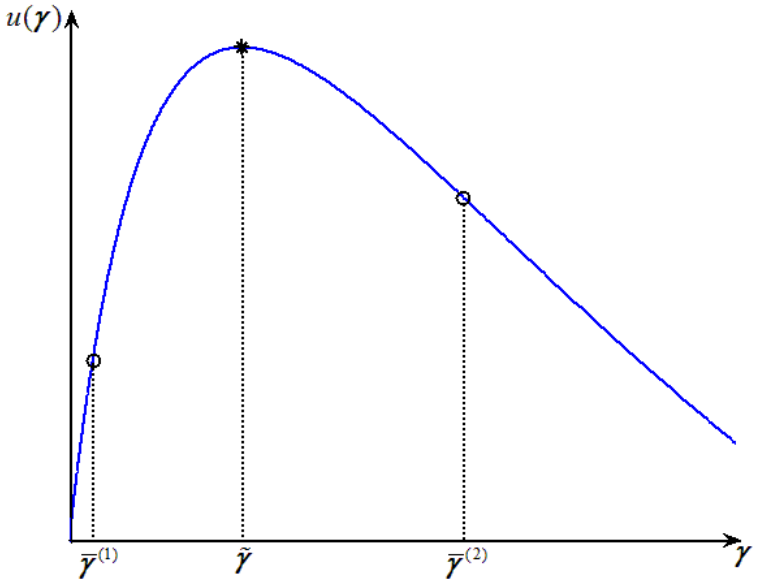

Figure 6. Generic shape of the utility as a function of the SINR for fixed interference.

denoting the SINR threshold corresponding to the minimum-GP specified by the QoS and

$$\tilde{\gamma}_q(\mathbf{p}_{-q}) = \Gamma\left\{\exp\left[\mathrm{W}\left(\frac{P_c\mu_q(\mathbf{p}_{-q})/\Gamma - 1}{\mathrm{e}}\right) + 1\right] - 1\right\}. \tag{14}$$

the SINR maximizing the EE function when constraints in problem (9) are neglected[‡].

Indeed, when $\mathbf{p}_{-q}$ is given, the optimal solution of the EE problem (9) simply consists in finding the power p_q that maximizes (6) subject to the QoS constraint. As shown in [12], $u_q(p_q|\mathbf{p}_{-q})$ is a quasi-concave function in p_q. Moreover, since there is linear dependence between γ_q and p_q, every property on γ_q holds for p_q too. Thus, the optimal solution in this case can be found as follows. First, the QoS constraint is neglected and the derivatives of $u_q(\cdot)$ w.r.t. to γ_q (or, equivalently, p_q) are studied, showing that $u_q(\cdot)$ takes the maximum in (14), which corresponds to the SINR value zeroing its first derivative. Then, since γ_q^* must be at least greater or equal $\bar{\gamma}_q$ in order to satisfy the QoS constraint, the optimal solution is given by (10)-(12).

Finally, before proceeding to the analysis of game (9), we provide here more insight on the meaning of the PC policy based on the EE approach, comparing it with the usual approach based on rate (or, SINR) satisfaction, e.g. [7, 9]. To this end, Fig. 6 depicts the generic shape of the utility function (6) vs. the SINR for a certain player, given a fixed interference caused by the other players. In particular, two QoS constraints, $\bar{\gamma}^{(1)}$ and $\bar{\gamma}^{(2)}$, are considered. In rate/SINR satisfaction PC schemes, the minimum power required to meet the QoS constraints with equality is allocated. Though, from an EE point of view, this may not be efficient. Indeed, as shown in Fig. 6, for $\bar{\gamma}^{(1)}$ the EE utility function would not be maximized. The EE based PC scheme instead, in order to minimize the waste of energy, allocates more power so that the optimal SINR results $\gamma^* = \tilde{\gamma} > \bar{\gamma}^{(1)}$, leading

[‡]The function $\mathrm{W}(\cdot)$ in (14) denotes the Lambert function, i.e., the function satisfying the equation $z = \mathrm{W}(z)\cdot\exp(\mathrm{W}(z)), \forall z \in \mathbb{C}$.

also to a rate higher than the minimum one. Obviously, when the QoS is such that the required SINR is greater than $\tilde{\gamma}$, as for $\bar{\gamma}^{(2)}$ in the example, then the EE and rate satisfaction approach returns the same result $\gamma^* = \bar{\gamma}^{(2)}$.

4.3. Game analysis and iterative solution

Capitalizing on Lemma 1, it readily follows that the GNE $\mathbf{p}^*$ must satisfy the best-response solution for each player [21], leading to the following proposition.

Theorem 1. *If problem (6) is feasible, then there exists an unique power allocation vector* $\mathbf{p}^* \triangleq [p_1^*, \cdots, p_Q^*]^T$ *that is the GNE of the game* $\mathcal{G}$*. The elements of* $\mathbf{p}^*$ *are the solutions to the following fixed-point system of equations:*

$$p_q^* = f_{\mathrm{BR}}\left(\mathbf{p}_{-q}^*\right) = \frac{\gamma_q^*(\mathbf{p}_{-q}^*)}{\mu_q(\mathbf{p}_{-q}^*)} \quad \forall q \in \mathcal{Q}, \tag{15}$$

where $\gamma_q^*(\mathbf{p}_{-q}^*)$ *is the optimal SINR obtained by replacing* $\mathbf{p}_{-q}$ *with* $\mathbf{p}_{-q}^*$ *in (12).*

The proof of Theorem 1 can be found in [12], while we summarize here some remarkable comments on it.

Feasibility. The feasibility of problem (9) can be checked following an approach similar to that adopted in [22]. If no upper bound on the power is considered, the feasibility amounts indeed to check whether there exists the vector $\bar{\mathbf{p}} = [\bar{p}_1, \cdots, \bar{p}_q]^T \geq \mathbf{0}$, such that $\gamma_q(\bar{\mathbf{p}}) = \bar{\gamma}_q$, $\forall q \in \mathcal{Q}$. This set of equations associated to the QoS constraint can be rearranged after some algebra as

$$(\mathbf{I} - \boldsymbol{\Upsilon})\,\bar{\mathbf{p}} = \mathbf{t}, \tag{16}$$

where $\boldsymbol{\Upsilon}$ is an $\mathbb{R}^Q \times \mathbb{R}^Q$ matrix whose (i,j)th element is

$$[\boldsymbol{\Upsilon}]_{i,j} = \begin{cases} 0 & i = j \\ \frac{\bar{\gamma}_q g_{i,j}}{g_{i,i}} & i \neq j \end{cases}, \tag{17}$$

and $\mathbf{t} = [\bar{\gamma}_1\sigma_1^2/|h_{1,1}|^2, \cdots, \bar{\gamma}_Q\sigma_Q^2/|h_{Q,Q}|^2]^T$. Then, as shown in [22], a necessary and sufficient condition for system (16) to have a solution (i.e., there exists $\bar{\mathbf{p}} \geq \mathbf{0}$ such that $\gamma_q(\bar{\mathbf{p}}) = \bar{\gamma}_q$, $\forall q \in \mathcal{Q}$) is that

$$\rho_{\boldsymbol{\Upsilon}} < 1, \tag{18}$$

where $\rho_{\boldsymbol{\Upsilon}}$ denotes the spectral radius of the matrix $\boldsymbol{\Upsilon}$. When also a maximum power constraint is set, problem (9) is feasible iff

$$\begin{cases} \rho_{\boldsymbol{\Upsilon}} < 1 \\ \bar{\mathbf{p}} = (\mathbf{I} - \boldsymbol{\Upsilon})^{-1}\,\mathbf{t} \leq \mathbf{p}^{(\max)}, \end{cases} \tag{19}$$

where $\mathbf{p}^{(\max)} \triangleq [p_1^{(\max)}, \cdots, p_Q^{(\max)}]^T$.

Existence. As shown in [12], the existence is ensured by analyzing the topological properties of the sets $\mathcal{P}_q$ expressed by (8) and showing that the objective function u_q is continuous and quasi-concave in $p_q, \forall q \in \mathcal{Q}$.

Uniqueness. Since the best-response $f_{\mathrm{BR}}(\cdot)$ is a standard function, the fixed-point system of equations (15) has an unique solution [23] and therefore the uniqueness of the underlying GNE is guaranteed.

Theorem 2. *If problem (9) is feasible, then the GNE $\mathbf{p}^*$ can be reached via an iterative algorithm based on the best response, wherein at each iteration ℓ, the power (i.e., the strategy) $p_q^{(\ell)}$ of every player is updated as*

$$p_q^{(\ell)} = f_{\mathrm{BR}}\left(\mathbf{p}_{-q}^{(\ell-1)}\right) = \frac{\gamma_q^*(\mathbf{p}_{-q}^{(\ell-1)})}{\mu_q(\mathbf{p}_{-q}^{(\ell-1)})}. \tag{20}$$

Moreover, the convergence is ensured starting from any initial power vector.

Proof. Since the best-response is a standard function, the iterative update of the power according to (20) is guaranteed to converge to the optimal point, i.e., the GNE $\mathbf{p}^*$, as demonstrated in [23].

The iterative algorithm based upon (20) is summarized in Tab. III, where $L_{\max}$ denotes the maximum number of iterations and ϵ the required accuracy interval, whereas the operator $\mathrm{LUT}(\cdot)$ selects the modulation order and coding rate based on the optimal SINR γ_q^*, as shown in Tab. II.

It is worth now to point out some considerations on the feasibility of the problem. Unlike most of the works on power control [7, 9], we here considered a maximum power level for transmission. When this constraint is not taken into account, the feasibility of the problem merely reduces to check if $\rho_{\boldsymbol{\Upsilon}} < 1$, otherwise checking the feasibility of the problem is equivalent to solve system (19). This can be done for instance at the gateway and adopted as an admission control mechanism before applying the iterative algorithm. When the problem is unfeasible it means that some or all beams may have capacities lower than traffic demands with available power, which may lead to traffic congestion for the system. As described in [24], solutions for this problem involve accepting more delay, possible data routing on alternate paths, and triggering transport layer congestion control mechanisms. Since congestion control policies are out of the scope of this analysis, in the following we consider the case where the problem is feasible.

However, since checking (19) may result more complex than only checking if $\rho_{\boldsymbol{\Upsilon}} < 1$, another possible approach, which entails accepting lower rates for some links, would be the following. The feasibility check is performed only according to (18) and, whenever this condition holds, the solution $\mathbf{p}^*$ is found as follows.

Corollary 1. *Given $\rho_{\boldsymbol{\Upsilon}} < 1$ and any initial starting power vector $\mathbf{p}^{(0)}$, the iterative algorithm, where at every iteration ℓ the power is updated as*

$$p_q^{(\ell)} = \min\left\{p_q^{(\max)}, f_{\mathrm{BR}}\left(\mathbf{p}_{-q}^{(\ell-1)}\right)\right\} = \min\left\{p_q^{(\max)}, \frac{\gamma_q^*(\mathbf{p}_{-q}^{(\ell-1)})}{\mu_q(\mathbf{p}_{-q}^{(\ell-1)})}\right\}, \quad \forall q \in \mathcal{Q}, \tag{21}$$

always converges to a unique fixed point.

Proof. Since $\bar{f}_{\mathrm{BR}} = \min\left\{p_q^{(\max)}, f_{\mathrm{BR}}\left(\mathbf{p}_{-q}^{(\ell-1)}\right)\right\}$ is still a standard function [23], then the iterative

Energy-efficient Resource Allocation Algorithm

Choose a feasible $p_q^{(0)} \in \mathbb{R}^+$, $\forall q \in \mathcal{Q}$, and set $\ell = 1$
Do
  For $q = 1, \cdots, Q$
    Compute $\hat{\mu}_q(\mathbf{p}_{-q}^{(\ell-1)})$ and $\gamma_q^*(\mathbf{p}_{-q}^{(\ell-1)})$
    Update $p_q^{(\ell)} = \frac{\gamma_q^*(\mathbf{p}_{-q}^{(\ell-1)})}{\hat{\mu}_q(\mathbf{p}_{-q}^{(\ell-1)})}$
    Set $\ell \leftarrow \ell + 1$
  End For
Until $||\mathbf{p}^{(\ell)} - \mathbf{p}^{(\ell-1)}|| \leq \epsilon$ or $\ell = L_{\max}$
Set $p_q^* = p_q^{(\ell)}$ and $(r_q^*, m_q^*) = \mathrm{LUT}(\gamma_q(p_q^*, \mathbf{p}_{-q}^*))$, $\forall q \in \mathcal{Q}$
Return p_q^*, (r_q^*, m_q^*), $\forall q \in \mathcal{Q}$

Table III

algorithm (21) is guaranteed to converge to a unique fixed point.

As anticipated, in this case there can be situations where at the end a player j converged to its maximum power but $\gamma_j(p_j^{(\max)}) < \bar{\gamma}_j$, i.e., the QoS constraint is not satisfied even at the maximum power. Anyway, as shown in [23], *i*) the power of those players that satisfy the QoS constraint is a feasible solution bounded above by the maximum power; *ii*) the other players that cannot achieve the required SINR threshold will continue to transmit at maximum power (or can be temporarily dropped by a scheduler).

5. SIMULATION RESULTS

In this section, the performance evaluation of the multibeam satellite downlink previously described is carried out by means of numerical simulations. As case of study, a Ka band GEO multibeam satellite with Europe-wide coverage is considered, composed of $N_{\mathrm{b}} = 60$ beams, each of $d = 170$ km of diameter, single feed per antenna [25] with $P_{\max} = 50$ W over 36 MHz bandwidth per transponder [26]. Considering a transponder's efficiency, defined as the ratio between the RF output power $P_{\max}$ and the DC input power P_c (supplied by the solar panels and batteries), of about 33% [26], the power consumption is set to $P_c = 150$ W. Fig. 7.a depicts the conventional four-color scheme here employed, where the Ka band is split in two contiguous subbands, termed B_1 and B_2, and both H and V polarizations are employed on both subbands; Fig. 7.b shows how the multibeam pattern, according to the color scheme just described, as been generated in simulation. The antenna

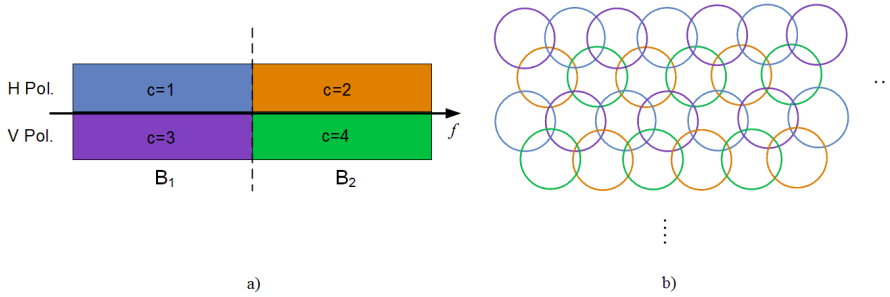

Figure 7. a) Color scheme and b) multibeam pattern used for numerical results.

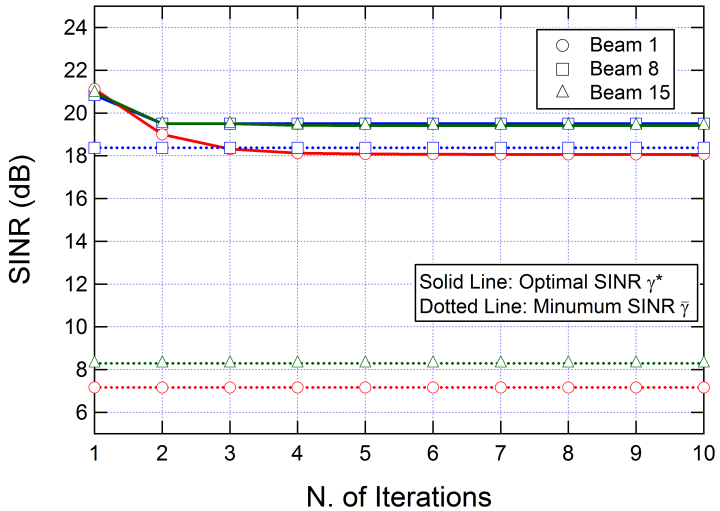

Figure 8. Optimal SINR vs. number of iterations.

gains $g_{i,j}$ are modeled according to the radiation pattern [27]

$$g_{i,j}(\theta) = G_{\max}\left(\frac{\mathrm{J}_1(\nu)}{2\nu} + 36\frac{\mathrm{J}_3(\nu)}{\nu^3}\right)^2, \tag{22}$$

where $\nu \triangleq 2.07123 \sin\theta / \sin\theta_{-3\mathrm{dB}}$, θ is the angle between the ith spot beam center and the jth UT location as seen from the satellite, $\theta_{-3\mathrm{dB}} = 0.2$, $G_{\max}|_{\mathrm{dB}} = 40$ dB is the maximum antenna gain, and $\mathrm{J}_1(\cdot)$ and $\mathrm{J}_3(\cdot)$ are the Bessel functions of the first kind and order 1 and 3, respectively. Recalling the single-frequency multibeam scenario described in Sect. 2.2, the position of each UT in every beam is randomly generated within a circle of radius $d/2$ centered in the relevant beam center. We will focus on the performance of the UTs belonging to a subset made of $Q = N_{\mathrm{b}}/C = 15$ beams denoted by the same color and labeled as beam q, with $q \in \{1, \cdots, 15\}$. The UTs are denoted by the following minimum-GP values $\bar{\boldsymbol{\eta}} = [2.2,\ 3.7,\ 1.5,\ 4.3,\ 5.2,\ 2.3,\ 1.2,\ 5.6,\ 4.3,\ 4,\ 2.7,\ 2.1,\ 2.2,\ 4.4,\ 2.5]$, expressed in bit/s/Hz, corresponding to the minimum SINR values $\bar{\boldsymbol{\gamma}} = [7.16,\ 12.39,\ 4.22,\ 14.32,\ 17.14,\ 7.54,\ 2.73,\ 18.37,\ 14.32,\ 13.36,\ 9,\ 6.77,\ \ 7.16,\ 14.64,\ 8.28]$, expressed in dB.

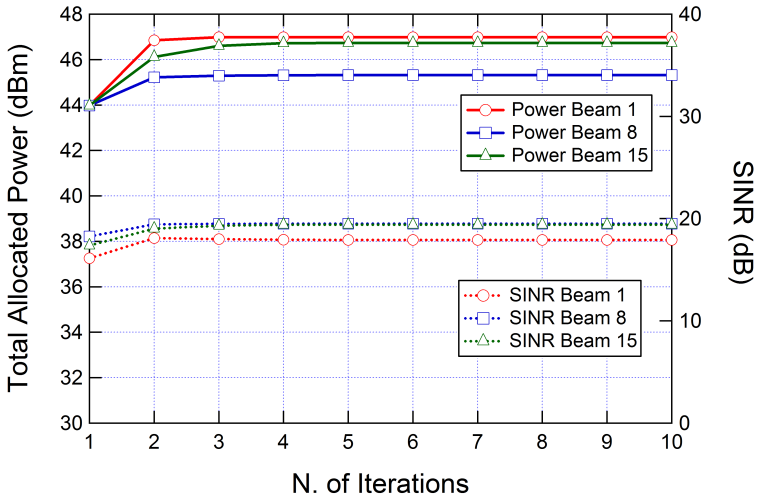

Figure 9. Power and SINR vs. number of iterations.

The main features of the proposed EE algorithm, i.e., efficiency, scalability and performance improvement compared to conventional rate satisfaction approaches, can be inferred from Figs. 8-12. For the sake of graph readability, results are shown for only a subset of the Q beams (i.e., beams 1, 8 and 15), but have general validity.

In detail, Fig. 8 depicts the minimum required SINR $\bar{\gamma}_q$ and compares this value with the optimal SINR γ_q^* at every iteration obtained applying the EE algorithm of Tab. III. The corresponding power p_q and actual SINR γ_q values at every iteration are shown in Fig. 9. As first remark, the efficiency of the EE algorithm is here apparent in that it converges in a few iterations (about 5) and, besides, at each iteration, the computation of the optimal power coefficient is in closed-form (20). Moreover, the performance improvement due to the EE approach clearly emerges. To this end, let us recall the main remarks pointed out at the end of Sect. 4.2. In the conventional approaches based on minimum rate satisfaction the power is chosen so that, at the end, every SINR γ_q matches the minimum one $\bar{\gamma}_q$ with strict equality, $\forall q \in \mathcal{Q}$. From an EE view point instead, the optimum power values p_q^*, i.e., the ones that maximize the EE (6), $\forall q \in \mathcal{Q}$, may be such that the SINR $\gamma_q > \bar{\gamma}_q$, in particular, $\gamma_q = \tilde{\gamma}_q$, $\forall q \in \mathcal{Q}$, according to (12). For instance, for beam 1 and 15, as shown in Fig. 8, the optimal SINR is much greater than the minimum one, and thus the allocated power is such that $\gamma_q = \tilde{\gamma}_q$, as can be seen from Fig. 9. This condition holds also for beam 8, even if this difference is less appreciable.

To corroborate this point, Fig. 10 depicts the value of the EE utility function (6) obtained when the power is allocated either with the EE strategy in Tab. III or with the minimum rate satisfaction strategy. It is worth to remark that the latter is obtained with the same approach adopted in Tab. III where, at every iteration ℓ, $\gamma_q^*(\mathbf{p}_{-q}^{(\ell)})$ is simply replaced with $\bar{\gamma}_q$. As expected, the EE function is maximized by the proposed approach. Only for beam 8, the value obtained for (6) is similar under both strategies, since, as previously seen, in this case $\bar{\gamma}_q \simeq \tilde{\gamma}_q$.

Poorly speaking, since at least an amount of power P_c is always employed, then the EE approach states that it may be more convenient to transmit with a power higher than the minimum one required to satisfy $\bar{\gamma}_q$ with equality. Employing an higher value of power thanks to the EE approach is also compliant with the perspective of adopting very high bandwidth efficient modulations, such 128-,

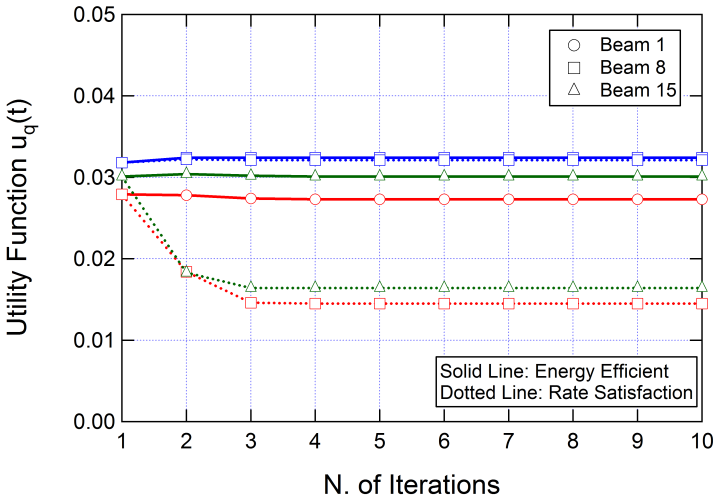

Figure 10. Energy Efficiency vs. number of iterations.

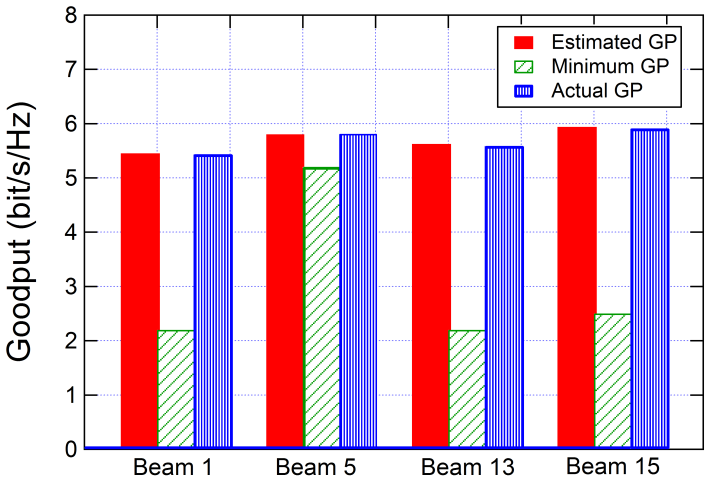

Figure 11. Average GP per Beam.

256-APSK, which requires an higher SINR value compared to modulations with lower order to have the same quasi-error free performance.

The performance improvement is also assessed in Fig. 11, which displays the GP obtained per UT for 4 out of Q beams under analysis. In particular, the first bar represents the estimated GP, obtained thanks to the EE algorithm, which returns γ_q^*, as $\eta_q^* = \log_2(1+\gamma_q^*/\Gamma)$, $\forall q \in \mathcal{Q}$. The second bar represents the minimum-GP constraint. The third bar instead denotes the actual GP, whose value is obtained by simulating the entire downlink transmission employing TM $(r_q^*, m_q^*) = \mathrm{LUT}(\gamma_q^*)$, $\forall q \in \mathcal{Q}$, i.e., pair modulation and coding rate selected plugging the optimal SINR into the ACM Tab. II. The latter values have been obtained averaging over 10^3 packet transmissions. The following comments are worth noting. The EE approach allows the GP of each user to increase w.r.t. the minimum required, since, in order to maximize the energy efficiency of the link, employs a higher

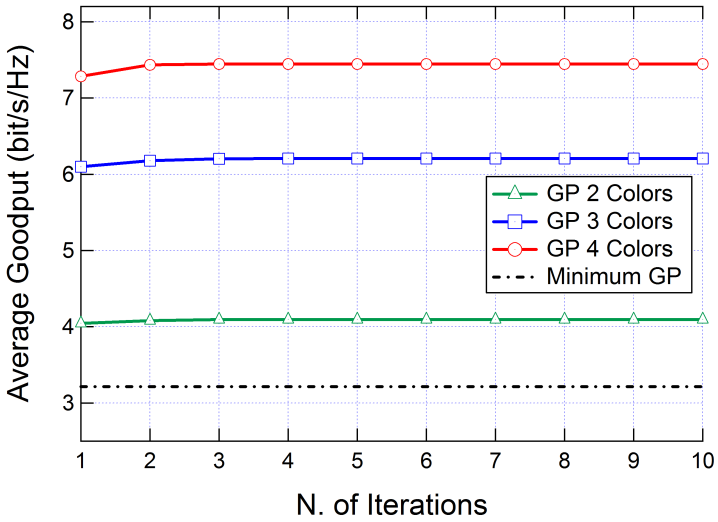

Figure 12. Average GP per Iteration for three different color schemes.

transmission power. Moreover, it can be seen that the estimated GP and actual GP are nearly the same, validating the approximation of the GP envelope of the static modes in Fig. 5 with eqn. (5).

Finally, Fig. 12 depicts how the average GP of $Q = 15$ iso-color beams varies in response to three different color schemes, i.e., 2, 3 and 4 colors, respectively. In every color scheme, the diameter of each beam is kept constant and equal to 170 km. The curves are obtained averaging the GP of the Q beams at every iteration. These curves are compared with the average minimum required GP. With 2-color scheme, the scenario is highly interference-limited, since the iso-color beams are closer to each other. As the number of colors increases, the mutual interference reduces, leading to a higher value of GP. It is worth to point out that usually, at least a 3-color scheme is employed [25], but also in the less practical 2-color scenario the proposed algorithm is able to improve performance with respect to the minimum required GP. Besides, the algorithm is adaptively scalable since, even in the worst condition of operability, i.e., with higher interference, converges within a few iterations.

6. CONCLUSIONS

This paper addressed the link resource allocation problem over the downlink of a multibeam Ka-band satellite, for packet data transmission towards ground-based terminals in a hybrid satellite/xDSL network. Channel varying conditions and the presence of interbeam interference caused by frequency/polarization reuse led to the following solutions. First, an effective ACM scheme, based on MC pairs of DVB-S2X standard which ensure very high spectral efficiency, was derived to obtain the pair yielding the highest value of GP for the actual SINR. Then, a centralized adaptive PC algorithm was also derived, maximizing the downlink EE under QoS constraint. Solution analysis of this PC problem was made resorting to the non-cooperative game theory. Numerical results derived for a realistic scenario revealed the efficiency and scalability of the proposed PC algorithm and that the resulting per-beam power setting fulfills the requirements

about QoS performance, showing also the advantages obtained w.r.t. conventional PC approached based on rate satisfaction.

ACKNOWLEDGEMENT

This work was supported by the European Commission in the framework of the FP7 Network of Excellence in Wireless COMmunications NEWCOM# (Grant agreement no. 318306).

REFERENCES

1. S. Egami, "A power-sharing multiple-beam mobile satellite in Ka band," *IEEE Journ. on Sel. Areas in Commun.*, vol.17, no.2, pp.145–152, Feb. 1999.
2. ETSI EN 302 307-2 V1.1.1, Digital Video Broadcasting (DVB); Second generation framing structure, channel coding and modulation systems for Broadcasting, Interactive Services, News Gathering and other broadband satellite applications. Part II: S2-Extensions (DVB-S2X), 2014.
3. R. Rinaldo, and R. De Gaudenzi, "Capacity analysis and system optimization for the reverse link of multi-beam satellite broadband systems exploiting adaptive coding and modulation," *Inter. Journ. of Sat. Commun. and Networ.*, vol 22, no. 4, pp. 425-448., July/Aug. 2004.
4. S. Cioni, R. De Gaudenzi, and R. Rinaldo, "Channel estimation and physical layer adaptation techniques for satellite networks exploiting adaptive coding and modulation", *Inter. Journ. of Sat. Commun. and Networ.*, vol 26, no. 2, pp. 157–188., Mar./Apr. 2008.
5. M.A. Vázquez-Castro, and G.S. Granados, "Cross-layer packet scheduler design of a multibeam broadband satellite system with adaptive coding and modulation," *IEEE Trans. on Wireless Commun.*, vol.6, no.1, pp. 248–258, Jan. 2007.
6. M. Angelone, A. Ginesi, E. Re, and S. Cioni, "Performance of a combined dynamic rate adaptation and adaptive coding modulation technique for a DVB-RCS2 system," *In Proc. of 6th. ASMS Conf. and 12th SPSC Workshop*, Sept. 2012.
7. J. Romero-García, and R. De Gaudenzi, "On antenna design and capacity analysis for the forward link of a multibeam power controlled satellite CDMA network," *IEEE Journ. on Sel. Areas in Commun.*, vol.18, no.7, pp.1230–1244, July 2000.
8. J. Lei, and M.A. Vázquez-Castro, "Joint power and carrier allocation for the multibeam satellite downlink with individual sinr constraints," *in Proc. IEEE Int. Conf. Commun.*, May 2010.
9. J. Lei, Z. Han, M.A. Vázquez-Castro, and A. Hjørungnes, "Secure Satellite Communication Systems Design With Individual Secrecy Rate Constraints," *IEEE Trans. Information Forensics and Security*, vol.6, no.3, pp. 661–671, Sept. 2011.
10. I. Stupia, V. Lottici, F. Giannetti, and L. Vandendorpe, "Link Resource Adaptation for Multiantenna Bit-Interleaved Coded Multicarrier Systems," *IEEE Trans. on Signal Process.*, vol. 60, no. 7, pp. 3644–3656, July 2012.
11. G. Miao, N. Himayat, G. Li, and S. Talwar, "Distributed interference-aware energy-efficient power optimization," *IEEE Trans. Wireless Commun.*, vol. 10, no. 4, pp. 1323–1333, Apr. 2011.
12. G. Bacci, E. V. Belmega, and L. Sanguinetti, "Distributed energy-efficient power optimization in cellular relay networks with minimum rate constraints," in *Proc. IEEE Intl. Conf. Acoustics, Speech and Signal Process. (ICASSP)*, Florence, Italy, May 2014.
13. D. Fudenberg, and J. Tirole, *Game Theory*. MIT Press: Cambridge, MA, 1991.
14. ETSI TS 102 771 V1.1, Digital Video Broadcasting (DVB); Generic Stream Encapsulation (GSE) implementation guidelines, 2011.
15. A. Mayer, B. Collini-Nocker, F. Vieira, J. Lei, and M.A. Vázquez Castro, "Analytical and Experimental IP Encapsulation Efficiency Comparison of GSE, MPE, and ULE over DVB-S2," *Intern. Workshop on Satellite and Space Commun. 2007 (IWSSC07)*, Sept. 2007.
16. G.D. Forney, and M.V. Eyuboglu, "Combined equalization and coding using precoding," *IEEE Commun. Mag.*, vol. 29, no. 12, pp. 25–34, Dec. 1991.
17. P.S. Chow, J.M. Cioffi, and J.A.C. Bingham, "A practical discrete multitone transceiver loading algorithm for data transmission over spectrally shaped channels," *IEEE Trans. on Commun.*, vol. 43, no. 2/3/4, pp. 773–775, Feb./March/April 1995.
18. S. Boyd, and L. Vandenberghe, *Convex Optimization*. Cambridge, U.K.: Cambridge Univ. Press, 2004.

19. E.M.T. Hendrix, and B.G.-Tóth, "Introduction to Nonlinear and Global Optimization", *Springer Optimization and Its Applications*, vol. 37, 2010.
20. C. U. Saraydar, N.B. Mandayam, and D. Goodman, "Efficient power control via pricing in wireless data networks," *IEEE Trans. on Commun.*, vol. 50, no. 2, pp. 291 – 303, Feb. 2002.
21. G. Scutari, D.P. Palomar, and S. Barbarossa, "Optimal Linear Precoding Strategies for Wideband Non-Cooperative Systems Based on Game Theory - Part I: Nash Equilibria", *IEEE Trans. on Signal Proc.*, vol. 56, no. 3, March 2008.
22. S. U. Pillai, T. Suel, and S. Cha, "The Perron-Frobenius theorem: some of its applications," *IEEE Signal Processing Magazine*, vol. 22, no. 2, pp. 62 – 75, March 2005.
23. R. D. Yates, "A framework for uplink power control in cellular radio systems," *IEEE Journal on Sel. Areas in Commun.*, vol. 13, no.7, pp. 1341–1347, Sep. 1995.
24. J. P. Choi, and V. W. S. Chan "Optimum Power and Beam Allocation Based on Traffic Demands and Channel Conditions Over Satellite Downlinks", *IEEE Trans. on Wireless Commun.*, vol. 4, no. 6, pp. 2983 – 2993, Nov. 2005.
25. M. Schneider, C. Hartwanger, and H. Wolf, "Antennas for multiple spot beam satellites", *CEAS Space Journal*, vol. 2, issue 1-4 , pp. 59–66, 2011–12.
26. B.R. Elbert, *The Satellite Communication Applications Handbook*. Artech House, Inc., MA, 2004. Boston
27. M.A. Diaz, N. Courville, C. Mosquera, G. Liva, and G.E. Corazza, "Non-Linear Interference Mitigation for Broadband Multimedia Satellite Systems," *Intern. Workshop on Satellite and Space Commun. 2007 (IWSSC07)*, Sept. 2007.